# NUMERICAL SIMULATION OF MODE I DELAMINATION BEHAVIOUR OF MULTIDIRECTIONAL COMPOSITE LAMINATES WITH FIBRE BRIDGING EFFECT

K. J. Wong[1,2*], X. J. Gong[1], S. Aivazzadeh[1], M. N. Tamin[2]

[1]*Département de Recherche en Ingénierie des Véhicules pour l'Environnement, Université de Bourgogne, Nevers, France*
[2]*Centre for Composites, Faculty of Mechanical Engineering, Universiti Teknologi Malaysia, Johor, Malaysia*
**jye1189@gmail.com*

**Keywords:** delamination, fracture toughness, fibre bridging, cohesive zone model.

**Abstract**
*In the present study, the R-curve behaviour of three different quasi-isotropic quasi-homogeneous composite laminates under mode I loading is simulated using cohesive zone model. Parametric studies are first carried out to investigate the effects of the interface strength, interface stiffness and element size to the response of the first lay-up. The optimised cohesive parameters are then used in the models of another two laminates. The results obtained indicate that for the case without fibre bridging, the bi-linear model is able to simulate the delamination behaviour accurately. For another two lay-ups with fibre bridging effect, the R-curve is included using tri-linear and exponential traction-separation laws. Results show that with proper selection of cohesive parameters and inclusion of R-curve effect, the delamination behaviour can be characterised well through numerical simulations.*

## 1 Introduction

Delamination is usually recognised as one of the earliest occurred failure modes in composite materials. Its initiation and propogation are characterised by fracture toughness and by R-curve, respectively. They are measured in most cases on unidirectional laminates. In multidirectional laminates, it is shown that the resistance to delamination depends strongly on the fibre orientation of adjacent plies. Hence, it is important to understand the delamination mechanisms in multidirectional laminates in order to predict the failure of a composite structure.

Gong et al. [1] reported that the variation of mode I fracture toughness, $G_{IC}$ across the width of the specimen depends not only on its staking sequence, but also on the initial crack length and specimen thickness to specimen width ratios. With this regard, to study the effects of fibre orientation to the delamination of the composites, several conditions have to be fulfilled. Besides, Pereira and de Morais [2] studied the mode I delamination behaviour of carbon/epoxy laminates with mid-plies of $0^o//\theta^o$. It was found that the adjacent fibre orientation has negligible effect on $G_{IC}$ values. However, higher $\theta^o$ value exhibits greater

resistance to the crack propagation, described by R-curve, where the formation of fibre bridging plays an essential rule.

In this study, the fibre bridging effect of carbon/epoxy composites with multidirectional fibre orientation under mode I loading through Double Cantilever Beam (DCB) test is studied numerically. Three 48-ply composite laminates are considered (Table 1), each with special stacking sequences that lead to uncoupled quasi-isotropic quasi-homogeneous (QIQH) property not only for the whole laminate, but also for each arm [3]. Symmetric laminate could ensure pure mode I delamination under DCB loading. For any 24-ply arm used here, the stiffness matrices $A_{ij}$, $D_{ij}$ and $B_{ij}$ are always the same and independent of the loading direction. In addition, even it is not symmetric, the coupling stiffness matrix **[B]** and the entries $A_{16}$, $A_{26}$, $D_{16}$ and $D_{26}$ in extensional **[A]** and bending **[D]** stiffness matrices could be eliminated. Moreover, for other entries, $A_{ij}$ is proportional to $D_{ij}$. This enables random selection of fibre orientation in the layers adjacent and sub-adjacent to the interface crack. Besides, the non-dimensional ratio $D_{12}^2/(D_{11}D_{22})$ is always equal to 0.1036.

| Nomenclature | Stacking sequence |
|---|---|
| [90/0//0/90] | [90/0/-45/45/-45/45/0/45/90/-45/90/0/90/0/45/0/-45/90/-45/45/-45/45/90/0]//sym |
| [-45/45//45/-45] | [-45/45/0/90/0/90/45/90/-45/0/-45/45/-45/45/90/45/0/-45/0/90/0/90/-45/45]//sym |
| [90/45//45/90] | [90/45/-45/0/-45/0/45/0/90/-45/90/45/90/45/0/45/-45/90/-45/0/-45/0/90/45]//sym |

* // refers to the location of the pre-crack.

**Table 1.** Stacking sequences of multidirectional laminates used in this study.

## 2 Modelling of fibre bridging effects

### *2.1 Modelling of bridging laws*

Figure 1 depicts the traction-separation relationship of tri-linear and exponential laws. The traction distribution of both laws is described in equation 1. The details of the tri-linear cohesive law could be found in the reference paper [4].

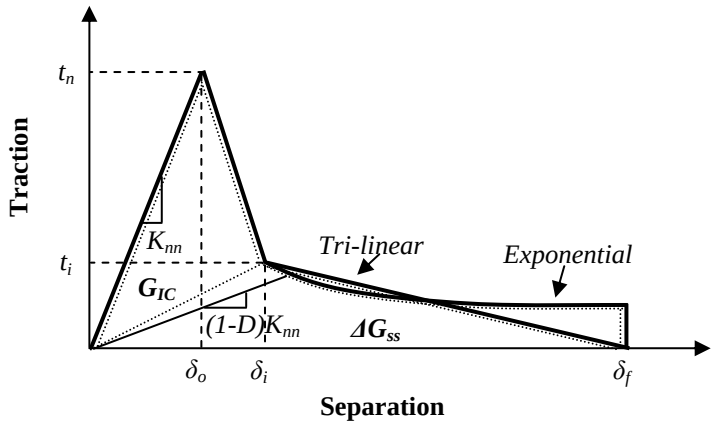


**Figure 1.** Traction-separation relationship of tri-linear and exponential bridging laws.

$$t=\begin{cases} K_{nn}\delta & \text{for } 0\le\delta\le\delta_o \\ t_n+t_i\dfrac{(\delta-\delta_o)}{(\delta_i-\delta_o)} & \text{for } \delta_o\le\delta\le\delta_i \\ \dfrac{2\Delta G_{SS}}{\delta_f(\delta_f-\delta_i)}(\delta_f-\delta) & \text{for } \delta_i\le\delta\le\delta_f \text{ (Tri-linear)} \\ \dfrac{\alpha\Delta G_{SS}}{(\delta_f-\delta_i)(1-\exp(-\alpha))}\left[\exp\left(-\alpha\dfrac{\delta-\delta_i}{\delta_f-\delta_i}\right)-1\right]+t_i & \text{for } \delta_i\le\delta\le\delta_f \text{ (Exponential)} \end{cases} \quad (1)$$

In this equation, $\delta$ is the crack opening displacement (COD) and $\alpha$ is the fitting parameter. Other parameters are as defined in Figure 1. In this study, the fitting parameter $\alpha$ is 2.4 and 0.8 for [-45/45//45/-45] and [90/45//45/90] lay-ups, respectively. With the above equations, the damage parameter *D* could be obtained as shown in equation 2.

$$D=\begin{cases} 1-\dfrac{t_i(\delta-\delta_o)}{K_{nn}\delta(\delta_i-\delta_o)}-\dfrac{\delta_o(\delta_i-\delta)}{\delta(\delta_i-\delta_o)} & \text{for } \delta_o\le\delta\le\delta_i \\ 1-\dfrac{t_i(\delta_f-\delta)}{K_{nn}\delta(\delta_f-\delta_i)} & \text{for } \delta_i\le\delta\le\delta_f \text{ (Tri-linear)} \\ 1-\dfrac{1}{K_{nn}\delta}\left\{\dfrac{\alpha\Delta G_{SS}}{(\delta_f-\delta_i)}\left[\dfrac{1-\exp\left(-\alpha\left(\dfrac{\delta-\delta_i}{\delta_f-\delta_i}\right)\right)}{1-\exp(-\alpha)}\right]+t_i\right\} & \text{for } \delta_i\le\delta\le\delta_f \text{ (Exponential)} \end{cases} \quad (2)$$

In these equations, damage value $D$=0 at $\delta=\delta_o$ and $D$=1 at $\delta=\delta_f$.

*2.2 Analysis of experimental R-curves*

The simulation works carried out in this study are based on the experimental results presented previously [5]. The assumption of interface crack profile that follows a third order polynomial as shown in Figure 2 [4], the COD $\delta$ could be estimated using equation 3.

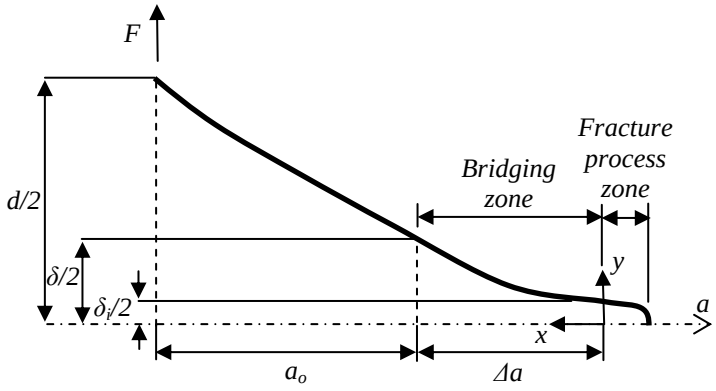


**Figure 2.** Assumed crack profile for a DCB specimen.

$$\delta=(d-\delta_i)\frac{\Delta a^2(2\Delta a+3a_o)}{(a_o+\Delta a)^3}+\delta_i \quad (3)$$

where $d$, $\Delta a$ and $a_o$ are the crack end displacement, increment in the crack length and initial crack length, respectively.

A drop in fracture energy of more than 5% from the previous maximum value is chosen as a basis for establishing representative R-curves. The sudden drop in fracture energy value is attributed to instable crack propagation. Thus, energy magnitude of lower than the previous attained maximum does not contribute to additional crack propagation. In fact, it is an energy storing process. The manipulated R-curves are then fitted with tri-linear [4] and exponential

laws, which could be obtained through the integral of the traction term. Equations 4 and 5 show the fitting equations for tri-linear and exponential laws, respectively.

$$dG = \frac{2\Delta G_{SS}}{\delta_f}\left\{\frac{\delta_i}{2} + \left[\frac{\delta_f(\delta-\delta_i) - \left(\frac{\delta^2-\delta_i^2}{2}\right)}{(\delta_f-\delta_i)}\right]\right\} \tag{4}$$

$$dG = \Delta G_{SS}\frac{1-\exp\left(-\alpha\frac{\delta-\delta_i}{\delta_f-\delta_i}\right)}{1-\exp(-\alpha)} + \left[t_i - \frac{\alpha\Delta G_{SS}}{(\delta_f-\delta_i)(1-\exp(-\alpha))}\right](\delta-\delta_i) \tag{5}$$

The term, *dG* represents an increment in the fracture energy.

The experimental and fitted R-curves for [-45/45//45/-45] and [90/45//45/90] lay-ups are shown in Figure 3 (CFRP composite with [90/0//0/90] lay-up does not show any R-curve effect). At least three experimental curves are taken for curve-fitting process. It is noted that there is a shift in the origin of different experimental curves, particularly in Figure 3(a). This is due to unavoidable crack jump that occurred at the start of crack propagation. Both bridging laws fit well the experimental data for the [-45/45//45/-45] lay-up. However, the exponential law fits the R-curves better than the tri-linear law for the [90/45//45/90] lay-up. It is observed that a single value of the fitting parameter $\alpha$ for the exponential law is capable of representing R-curve data with various shapes.

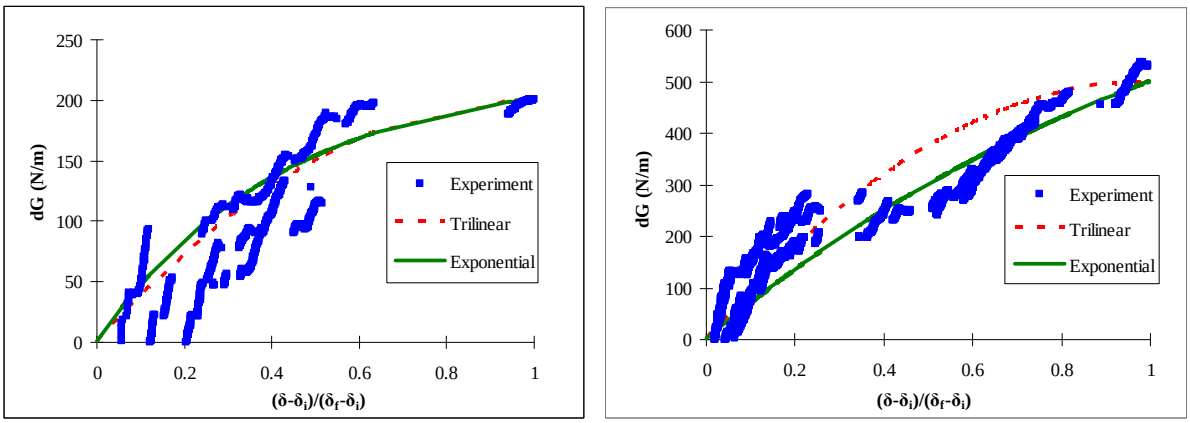


**Figure 3.** Experimental and fitted R-curves for (a) [-45/45//45/-45] and (b) [90/45//45/90] lay-ups.

## 3 Numerical modelling

### *3.1 Finite element model*

Figure 4 shows the geometry of the finite element model along with loading and boundary conditions used in this study. The adjacent two upper and lower plies to the mid-plane and their interfaces are explicitly modelled. Each of these four plies is modelled using continuum shell elements (SC8R) with prescribed Hashin's damage model. Cohesive elements with matching nodes (COH3D8) are prescribed for interfaces between these plies. Other plies are modelled as equivalent composite layer with three elements in thickness direction. These two equivalent layers are discretised with biased mesh towards the mid-plane, as illustrated in Figure 4. Properties of plies and interfaces used in the simulation are listed in Table 2.

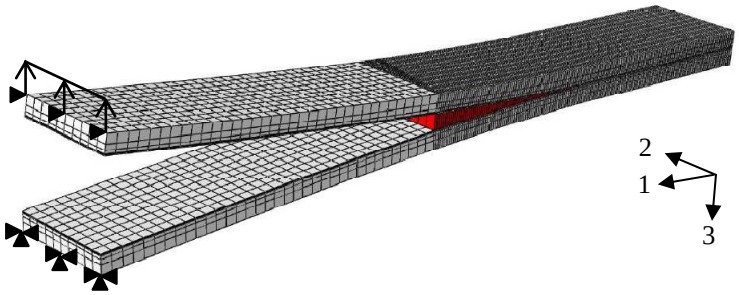


**Figure 4.** The finite element model used in this study.

| $E_1$ (GPa) | $E_2$ (GPa) | $G_{12}$ (GPa) | $G_{13}$ (GPa) | $G_{23}$ (GPa) | $v_{12}$ |
|---|---|---|---|---|---|
| 103 | 7 | 3.15 | 3.15 | 2.75 | 0.34 |

| $X^T$ (MPa) | $X^C$ (MPa) | $Y^T$ (MPa) | $Y^C$ (MPa) | $S^L$ (MPa) | $S^T$ (MPa) | $G_{mc}$ (N/mm) | $G_{fc}$ (N/mm) |
|---|---|---|---|---|---|---|---|
| 1688 | 1500 | 41 | 140 | 65 | 32.5 | 0.5 | 1.5 |

| $K_{nn}$ ($N/mm^3$) | $t_n$ (MPa) | $G_{IC,0/90}$ (N/mm) | $G_{IC,\pm45}$ (N/mm) | $G_{IC,45/90}$ (N/mm) |
|---|---|---|---|---|
| $5x10^3$ | 25 | 0.4734 | 0.4973 | 0.4426 |

**Table 2.** Material and interface properties of the lamina and the interface.

## 3 Results and discussion

### *3.1 Effects of cohesive parameters*

Parametric studies of cohesive parameters are performed using only CFRP composite laminate with [90/0//0/90] lay-up. It is because this particular lay-up does not show any fibre bridging effect. The optimised cohesive parameters obtained are then used for modelling the response of the other two specimens with different lay-ups.

#### *3.1.1 Effects of interface strengths*

Figure 5 shows effects of different interface strengths ranging from 5–55 MPa to the force-displacement response of the composites. Results indicate that for composites with high interface strengths ($t_n$=40 and 55 MPa), a significant increment in the peak load is predicted.

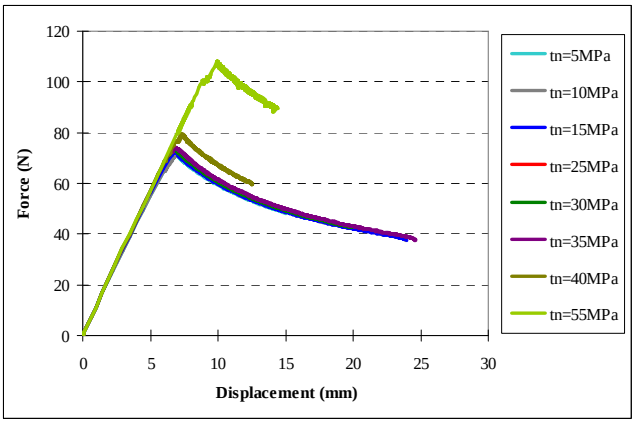


**Figure 5.** Effects of interface strengths on the force-displacement response.

*3.1.2 Effects of interface stiffness*

Results shown in Figure 6 indicate that the favourable interface stiffness should range between $5x10^3$ and $1x10^6$ N/mm$^3$. At low stiffness ($K_{nn}$=$1x10^3$ N/mm$^3$), the peak load is over-predicted while at high value ($K_{nn}$=$1x10^7$N/mm$^3$), the curve deviates in the damage propagation region.

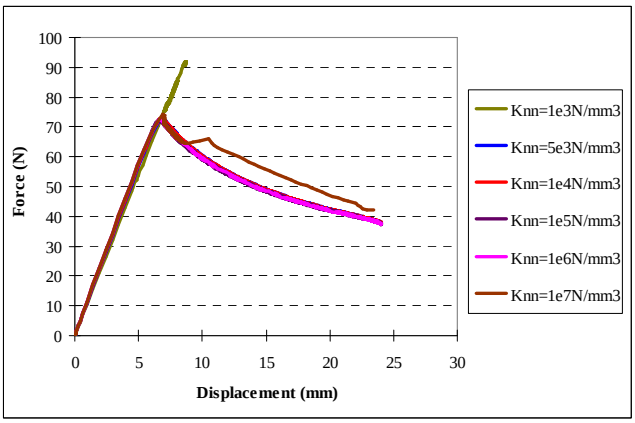


**Figure 6.** Effects of interface stiffness on the force-displacement response.

*3.1.3 Effects of element size*

Results shown in Figure 7 indicate that element sizes $l_e$ of 1.5 and 2 mm lead to significant fluctuation in the crack propagation region. The curves show negligible oscillation for $l_e \leq 1$ mm.

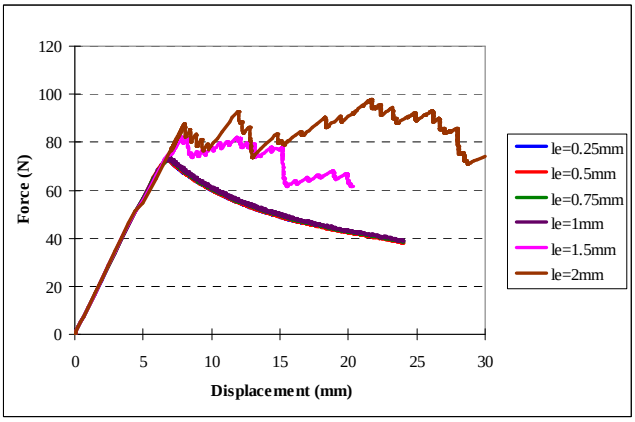


**Figure 7.** Effects of element size on the force-displacement response.

Based on the results from parametric studies, subsequent numerical models are performed with $t_n$=25 MPa, $K_{nn}$=$1x10^4$ N/mm$^3$ and $l_e$=0.5 mm. These parameters ensure that there are four elements in the cohesive zone length.

*3.2 Comparison between traction-separation laws*

Figures 9-11 show comparison of experimental and numerical force-displacement curves of the laminates with three different stacking sequences. As observed from Figure 9, the bi-linear model simulates well the response of [90/0//0/90] lay-up, which does not show any fibre bridging effect. The predicted initial slope and the peak load are very similar to measured values (less than 5% difference). In the damage propagation region, the numerical curve is slightly higher than experimental values. As for the laminate with mid-plies of [-45/45//45/-

45], both tri-linear and exponential models predict well the force-displacement (Figure 10). The force-displacement curve without fibre bridging effect ($G_c$=$G_{IC}$) is included for comparison. The effect of R-curve is not significant because the increment in the fracture toughness $\Delta G_{SS}$, is only about 40% of the $G_{IC}$ value. The force-displacement curve obtained using bi-linear model at fracture energy equals to the steady-state value ($G_C$=$G_{SS}$) signifies an over-prediction. Improvement in the R-curve effect based on numerical simulation results is clearer in the [90/45//45/90] lay-up, where $\Delta Gss \approx 1.4 G_{IC}$. The curve in the crack propagation region is "raised" when compared to the numerical response without fibre bridging effect. Again, for the case where $G_C$=$G_{SS}$, the curve is over-predicted. In addition, in the damage propagation region, the tri-linear model curve over-predicts the exponential curve, which conforms to the fitted curves shown in Figure 2(b). Furthermore, the numerical peak loads and slopes in Figures 10 and 11 are generally lower compared to the experimental values, with a maximum of 14% difference. This could be due to the resin rich region and the variation in the thickness of the specimens.

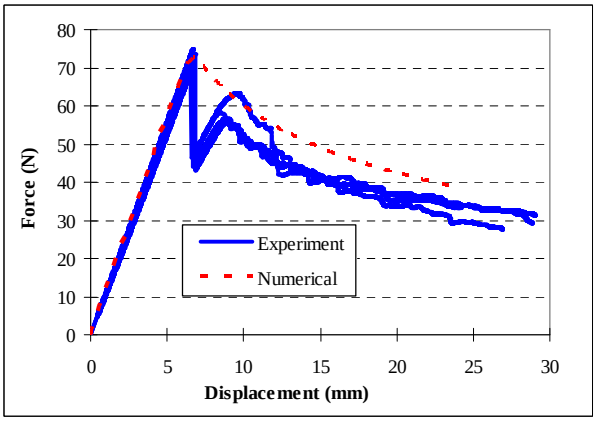


**Figure 9.** Experimental and numerical force-displacement curves of [90/0//0/90] lay-up.

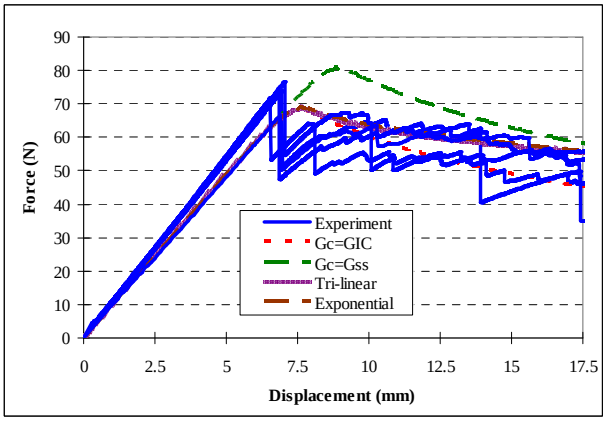


**Figure 10.** Experimental and numerical force-displacement curves of [-45/45//45/-45] lay-up.

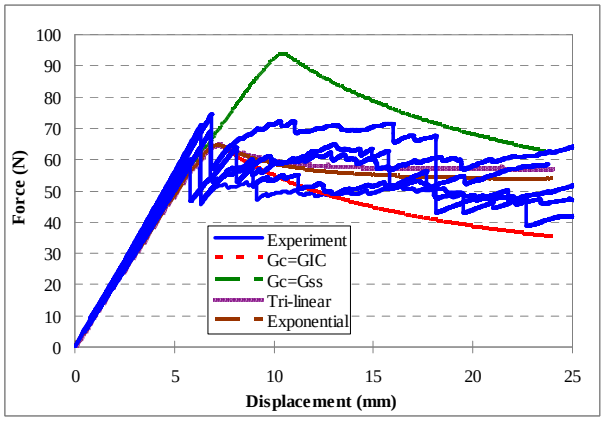


**Figure 11.** Experimental and numerical force-displacement curves of [90/45//45/90] lay-up.

## 4 Conclusions

Delamination behaviour of three different QIQH carbon/epoxy composite laminates under DCB Mode I loading has been examined numerically. Results show that the numerical models response well with interface traction between 5-35 MPa, interface stiffness in the range of $5x10^3$-$1x10^6$ N/mm$^3$ and element size of 1 mm and below. Four elements are needed in the cohesive zone length to ensure accurate modelling results. Besides, fibre bridging effect could be modelled using tri-linear and exponential traction-separation laws. However, the exponential law gives a higher flexibility in the curve-fitting through the parameter $\alpha$ in the equation.

## References

[1] Gong X.J., Hurez A., Verchery G. On the determination of delamination toughness by using multidirectional DCB specimens. Polymer Testing, **29**, pp. 658-666 (2010).

[2] Pereira A.B., de Morais A.B. Mode I interlaminar fracture of carbon/epoxy multidirectional laminates. *Composites Science and Technology*, **64**, pp. 2261-2270 (2004).

[3] Vannucci P., Verchery G. A new method for generating fully isotropic laminates. *Composite Structures*, **58**, pp. 75-82 (2002).

[4] Gutkin R., Laffan M.L., Pinho S.T., Robinson P., Curtis P.T. Modelling the R-curve effect and its specimen-dependence. *International Journal of Solids and Structures*, **48**, pp. 1767-1777 (2011).

[5] Mohamed Rehan M.S., Rousseau J., Gong X.J., Ali J.S.M. Effects of fiber orientation of adjacent plies on the mode I crack propagation in a carbon-epoxy laminates. *Procedia Engineering*, **10**, pp. 3179-3184 (2011).